Optimal Operation of Solar Battery Chargers via Mixed-Integer Linear Programming

Gianni Bianchini, *Member, IEEE*, Marco Casini, *Senior Member, IEEE*, Antonino Laudani, *Member, IEEE*, and Gabriele Maria Lozito, *Member, IEEE*

***Abstract*—This letter considers an islanded system consisting of a photovoltaic source connected to a battery storage through power converters, subject to a time varying load. An innovative charging architecture composed of two DC-DC converters and a super-capacitor is considered, and a novel modeling and optimal control framework is proposed with the aim of optimizing battery charge/discharge cycles while satisfying given generation and load profiles. Nonlinearities and nonconvex constraints arising from the electrical models are suitably treated in order to devise an optimal control problem involving linear dynamics that can be solved to the global optimum via mixed-integer linear programming. Numerical simulations based on a real data set show the effectiveness of the proposed approach as well as its computational feasibility.**

***Index Terms*—Solar energy, electrical storage systems, optimal control.**

I. Introduction

IN RECENT years, photovoltaic (PV) generation systems have undergone an extraordinary development and have become a leading technology for renewable energy production. To fully exploit their potential, it is common practice to combine them with energy storage systems (ESSs). Such a combination is exploited to allow the energy surplus to be used when solar power is unavailable, as well as to balance grid operation and increase its stability [1], [2]. Electrical storage devices fall into two main categories: batteries, with lithium-ion batteries being the prominent technology, and super-capacitors (SCs). Batteries are characterized by high energy density but low power density, and are prone to performance degradation when subjected to repeated charge/discharge cycles; on the other hand, SCs exhibit low energy density and high power density, are generally more durable and more resilient to high current rates and variable load conditions. The complementarity of these two classes of devices led to the proposal of hybrid solutions where SCs and batteries cooperate to compensate for each other's shortcomings [3].

In this letter, we consider a recently introduced direct current (DC) charger architecture [4] based on the cascade of two DC-DC converters decoupled by an SC. In this architecture, a first converter is used to control the operating point of the PV device, which is required, e.g., to achieve Maximum Power Point Tracking (MPPT) and/or compensation for partial shading conditions [5], [6]. A second converter is used for regulating the battery current, while the introduction of an SC acting as both a DC link and an auxiliary storage allows for absorbing rapid current variations during transients. This reduces stress on the battery, thus preventing premature degradation and preserving its overall capacity. A similar framework is proposed in [7]. A key characteristic of this charger architecture is the flexibility offered by the two converter gains, which can be exploited as control variables to regulate, e.g., both the operating point of the PV source and the battery charging/load current. In [7], this feature is exploited via an empirical control scheme based on PID and fuzzy logic in order to achieve MPPT on the PV side and constant current charging on the battery side. A prominent shortcoming of such an approach is that the existence of loads is not accounted for, i.e., the analysis is limited to the charging process. The presence of loads is inescapable in several application contexts such as microgrids, and in this case the combined battery charging/discharging behavior must be explicitly accounted for, as it represents the main source of battery degradation [8]. The latter should be minimized due to economic and environmental reasons. Moreover, numerous constraints arise in the overall system, including, e.g., PV power availability depending on weather, battery capacity and safety bounds, charging/discharging current limitations, and operating ranges of the electrical components. The above requirements call for the development of a suitable optimal control framework, possibly relying on formulations that can be solved to the global optimum and in a computationally feasible manner. This is not a straightforward task due to the

Received 17 March 2025; revised 5 May 2025; accepted 19 May 2025. Date of publication 26 May 2025; date of current version 5 June 2025. This work was supported by the European Union Next Generation EU, Mission 4, Component 1, through Project MOST4BIPV under Grant CUP: B53D23023820001. Recommended by Senior Editor S. Baldi. *(Corresponding author: Marco Casini.)*

Gianni Bianchini and Marco Casini are with the Dipartimento di Ingegneria dell'Informazione e Scienze Matematiche, Università di Siena, 53100 Siena, Italy (e-mail: giannibi@diism.unisi.it; casini@diism.unisi.it).

Antonino Laudani is with the Dipartimento di Ingegneria Elettrica, Elettronica e Informatica, Università di Catania, 95123 Catania, Italy (e-mail: alaudani@unict.it).

Gabriele Maria Lozito is with the Dipartimento di Ingegneria dell'Informazione, Università di Firenze, 50139 Firenze, Italy (e-mail: gabrielemaria.lozito@unifi.it).

Digital Object Identifier 10.1109/LCSYS.2025.3573333

nonlinear nature of the involved dynamics and nonconvexity of the constraints.

In this letter, we aim at filling the above research gap by providing the contributions summarized below.

- An optimal strategy for scheduling the operation of the considered architecture under variable loads and weather conditions is designed, with the aim of optimizing the battery charging cycles while satisfying generation, load, and technological constraints;
- An optimal control scheme underpinning such strategy is developed making use of standard nonlinear models of both PV generation and battery storage. The most notable feature of such scheme is that nonlinearities in the dynamics and nonconvex constraints arising from the electrical models are suitably treated so that the optimal control problem involves linear dynamics and can be solved to the global optimum via a low-complexity mixed-integer linear program (MILP).

The proposed control strategy is validated through numerical simulations based on realistic devices and weather data taken from [9]. The performance of the devised control technique is compared to that of an adaptation (due to the presence of load and physical constraints) of the standard MPPT operation combined with constant current charging, showing the superiority of the proposed approach in optimizing battery life while maintaining a minimal computational effort.

The letter is organized as follows: the models of the components of the considered setup are introduced in Section II. In Section III, the proposed optimal control strategy is derived. Numerical simulations are provided in Section IV, while conclusions are drawn in Section V.

II. System Modeling

In this section, the models used to represent the full energy conversion chain are presented.

A. Photovoltaic Source

The electrical equivalent model of a PV source that will be used throughout this letter is the widely adopted single-diode model [10]. The electrical behavior is completely regulated by the voltage-current relationship given by (see Fig. 1)

$$i_{pv} = I_{irr} - I_o\left[e^{\frac{v_{pv}+R_s i_{pv}}{N_s n V_T}} - 1\right] - \frac{v_{pv}+R_s i_{pv}}{R_{sh}}, \qquad (1)$$

where V_T denotes the thermal voltage, N_s is the number of series connected PV cells, I_{irr} is the photocurrent, I_o is the diode reverse saturation current, n is the diode ideality factor, R_s is the series resistance, and R_{sh} is the shunt resistance.

The previous parameters depend on irradiance G and/or temperature of the cell T_c [10]. Equation (1) can be solved through iterative methods or via the Lambert-W function to derive the PV voltage v_{pv} for a known PV current i_{pv} or vice versa [11], and also to determine, given G and T_c, the maximum power operation point (MPP) of the PV source

$$P_{MPP} = \max_{(v_{pv},i_{pv}) \text{ in } (1)} P_{pv},$$

with $P_{pv} = v_{pv} i_{pv}$. Another well-known feature captured by the model in (1) is that a given reference power $P_{pv} < P_{MPP}$ can

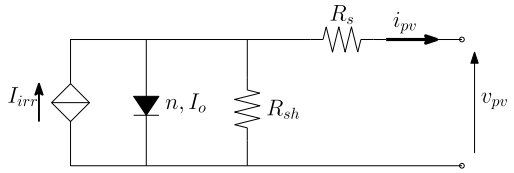

Fig. 1. Single diode model for a silicon photovoltaic device.

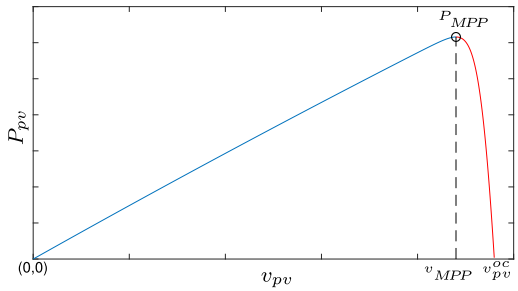

Fig. 2. Voltage-power characteristics of a solar cell. The blue curve denotes the operating points $(v_{pv}^-[P_{pv}], i_{pv}^-[P_{pv}])$, while the red one represents $(v_{pv}^+[P_{pv}], i_{pv}^+[P_{pv}])$.

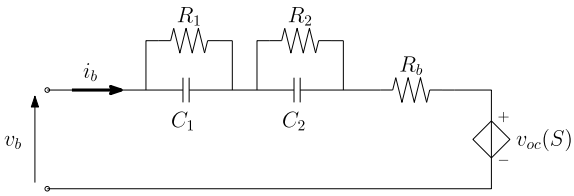

Fig. 3. Dynamic model of the battery.

be tracked at two different operating points $(v_{pv}^-[P_{pv}], i_{pv}^-[P_{pv}])$ and $(v_{pv}^+[P_{pv}], i_{pv}^+[P_{pv}])$, see Fig. 2, which can be computed numerically. In the framework considered in this letter, it is convenient to operate the PV panel at $(v_{pv}^+[P_{pv}], i_{pv}^+[P_{pv}])$. In that region, the PV voltage v_{pv} is always greater or equal to the MPP voltage v_{MPP} and close to the open circuit voltage v_{pv}^{oc}, see [11].

B. Battery

The battery model employed in this letter consists of a nonlinear voltage source with series resistance and two RC cells that account for rapid transient phenomena such as charge diffusion processes [12]. This model (see Fig. 3) is used to represent a large variety of cells of different technologies [13]. The state of charge (SOC) S, which represents a continuous state variable of the battery model, belongs to the closed interval $[0, 1]$.

The full state equation model is expressed as

$$\dot{S} = \frac{1}{Q_N} i_b, \quad \dot{v}_{C_i} = \frac{1}{C_i}\left[i_b - \frac{v_{C_i}}{R_i}\right], \ i = 1, 2 \qquad (2)$$

where Q_N is the nominal capacity of the battery.

In lithium-ion batteries, the open circuit voltage v_{oc} is a nonlinear function of S. In this letter, we consider the model developed in [14], given by

$$v_{oc}(S) = a_1 e^{b_1 \cdot S} - a_2 e^{b_2 \cdot S} + v^{cut}, \qquad (3)$$

where parameters a_1, a_2, b_1, b_2 depend on battery quality and aging, while v^{cut} is a constant termed cut-off voltage. In Fig. 4,

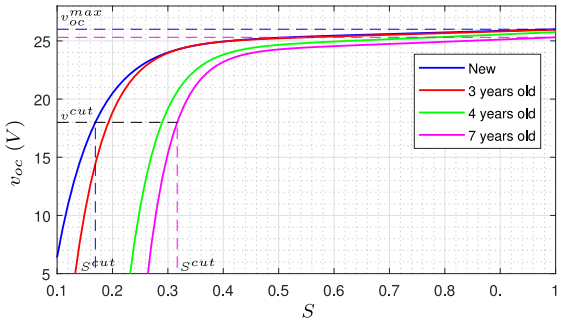

Fig. 4. Battery open circuit voltage v_{OC} vs. state of charge S for lithium-ion batteries of different age. Parameters v^{cut}, v_{oc}^{max} and S^{cut} are reported for a new battery and a 7-year-old battery.

the plot of v_{oc} vs. S is reported for an ESS system consisting of the parallel of 2 series of 9 batteries with the parameters reported in [14], for different battery aging.

Remark 1: Rechargeable batteries are in general not meant to be fully discharged, since a full discharge can permanently damage them, and operation below v^{cut} must not be allowed to avoid overdischarging [14]. This condition requires enforcing a lower bound $v_{oc}^{min} \geq v^{cut}$ on v_{oc}, corresponding via (3) to a lower bound $S^{min} \geq S^{cut} = \log(a_1/a_2)/(b_2 - b_1)$ on S. An upper bound v_{oc}^{max} can be similarly imposed. Taking $v_{oc}^{max} = v_{oc}(1)$, corresponding to a fully charged battery, and $v_{oc}^{min} = v^{cut}$, i.e., the largest interval $[v_{oc}^{min}, v_{oc}^{max}]$, the ratio $v_{oc}^{min}/v_{oc}^{max}$ for common devices varies in the range $[0.77, 0.79]$, corresponding to S^{min} varying in $[0.17, 0.32]$, over $[0, 7]$ years of battery age [14], [15] (see Fig. 4). Narrower limits $[v_{oc}^{min}, v_{oc}^{max}]$ are used to improve battery life. Such limitations are typically enforced via the device circuitry.

C. DC-DC Converters

All DC-DC converters are switched circuits that require time-domain modelling with time steps well below the time constants involved in the charging process of the battery. For this reason, it is common to consider the DC-DC converters at steady-state [16], [17]. In this case, the converter can be seen as a DC transformer, for which it is possible to define a voltage gain M_v and a current gain M_i such that

$$M_v = v_o/v_i, \quad M_i = i_o/i_i. \tag{4}$$

For the sake of simplicity, we neglect any loss associated to either parasitic components or switching, and so $M_v M_i = 1$.

D. Double Conversion Stage Battery Charger

In this letter, we consider a double conversion stage composed of two first order (buck, boost) converters in cascade with a DC bus consisting of a suitably dimensioned supercapacitor. This configuration is in general referred to as *split-π* [4], [18], [19]. The load is modeled through an ideal current generator connected to the output terminals of the boost converter. Since the dynamics of the charging process is much slower than the charge diffusion on the battery, capacitors C_1 and C_2 in Fig. 3 can be neglected. Thus, the schematic representation of the overall system can be illustrated as in Fig. 5, where $R = R_1 + R_2 + R_b$ is the overall resistance of the battery and i_l denotes the load current. Let us

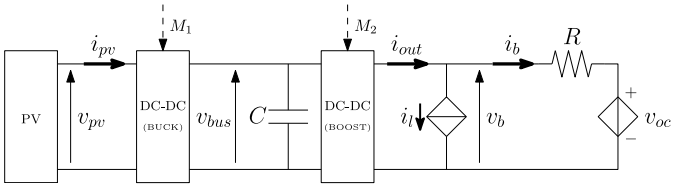

Fig. 5. Double conversion stage model.

denote by $M_1 < 1$ and $M_2 > 1$ the voltage gains of the buck and boost converters, and by P_{pv} and P_l the PV generation and load power, respectively. Then, according to (2) and (4) the overall system can be modeled as

$$\dot{S}(t) = \frac{1}{Q_N} i_b(t) \tag{5a}$$

$$\dot{v}_{bus}(t) = \frac{1}{C}\left[\frac{1}{M_1(t)} i_{pv}(t) - M_2(t) i_{out}(t)\right], \tag{5b}$$

where

$$v_{bus}(t) = M_1(t) v_{pv}(t) \tag{6}$$

$$i_b(t) = \frac{1}{R}(M_2(t) v_{bus}(t) - v_{oc}(S(t))) \tag{7}$$

$$i_{out}(t) = i_b(t) + \frac{P_l(t)}{M_2(t) v_{bus}(t).} \tag{8}$$

Notice that (5b) represents the voltage dynamics of the SC with equivalent capacity C. In the above nonlinear model, the converter gains $M_1(t)$ and $M_2(t)$ constitute the command inputs to the system.

III. Optimal Control Design

In this section, an optimal control strategy is derived for the considered solar charger model in order to schedule the charging process over a given time horizon (e.g., one day) under a variable load, with the aim of optimizing the battery charging cycles while satisfying generation, load, and device operational constraints. The proposed approach is based on suitable manipulations of the models in Section II and of the corresponding constraints, so that the underlying optimization problem boils down to a low-complexity MILP, which can be efficiently solved to the global optimum.

Since the PV generator power is given by $P_{pv}(t) = v_{pv}(t) i_{pv}(t)$, by substituting (6)-(8) into (5b), the system state equations can be rewritten as

$$\dot{S}(t) = \frac{1}{Q_N} i_b(t) \tag{9a}$$

$$\dot{v}_{bus}(t) = \frac{P_{pv}(t) - i_b(t)(R i_b(t) + v_{oc}(S(t))) - P_l(t)}{C v_{bus}(t)}, \tag{9b}$$

and moreover

$$M_1(t) = \frac{v_{bus}(t)}{v_{pv}(t)} \tag{10a}$$

$$M_2(t) = \frac{R i_b(t) + v_{oc}(S(t))}{v_{bus}(t)}. \tag{10b}$$

Using the SC bus stored energy

$$E_{bus}(t) = \frac{1}{2} C v_{bus}^2(t) \tag{11}$$

as a state variable in (9b) in place of $v_{bus}(t)$, it is easily seen that the system dynamics can be further expressed as that of

two integrators, i.e.,

$$\dot{S}(t) = \frac{1}{Q_N} u_1(t) \tag{12a}$$

$$\dot{E}_{bus}(t) = u_2(t) - P_l(t), \tag{12b}$$

where the auxiliary control inputs $u_1(t)$, $u_2(t)$ are given by

$$u_1(t) = i_b(t) \tag{13a}$$

$$u_2(t) = P_{pv}(t) - R u_1^2(t) - v_{oc}(S(t)) u_1(t). \tag{13b}$$

Clearly, $M_1(t)$ and $M_2(t)$ can be recovered from $u_1(t)$ and $u_2(t)$ by computing $P_{pv}(t)$ from (13b), and in turn $v_{pv}(t) = v_{pv}[P_{pv}(t)]$ numerically as pointed out in Section II-A, and finally using (11) in (10).

Discretizing (12) via the Zero-Order-Hold (ZOH) equivalent method with sampling time τ_s, and denoting by the subscript k the sampling of a variable $(\cdot)(t)$ at the k-th time step, i.e., $(\cdot)_k = (\cdot)(k\tau_s)$, $k = 0, 1, \ldots,$ one gets

$$S_{k+1} = S_k + \frac{\tau_s}{Q_N} u_{1,k} \tag{14a}$$

$$E_{bus,k+1} = E_{bus,k} + \tau_s u_{2,k} - \tau_s P_{l,k}. \tag{14b}$$

The sought optimal control problem is formulated over a discrete time horizon $k \in \mathcal{T}$, $\mathcal{T} = 0, 1, \ldots, T$. In such formulation, it is assumed that $P_{l,k}$ and $P_{MPP,k}$ represent forecasts of the load and peak PV power, respectively, where the latter is in turn computed on the basis of a weather forecast $(G_k, T_{c,k})$ as outlined in Section II-A. Such forecasts are assumed to be available at the beginning of the control horizon. The following constraints are enforced on the control system variables in order to account for technological and performance limitations of the models.

- *PV power.* PV generation, which in turn determines the operating point of the PV device at each time step as outlined above, must be kept between 0 and the maximum available power forecast, i.e.,

$$0 \le P_{pv,k} \le P_{MPP,k}. \tag{15}$$

- *Battery current and SOC.* Charge/discharge current i_b must satisfy suitable technological bounds for proper device operation that is,

$$i_b^{min} \le u_{1,k} \le i_b^{max}, \tag{16}$$

where $i_b^{min} < 0$ and $i_b^{max} > 0$. In general, the battery discharge current must be kept considerably lower than the short circuit current $v_{oc}(S)/R$, and therefore it can be assumed without loss of generality that

$$|i_b^{min}| \le \frac{v_{oc}^{min}}{2R}. \tag{17}$$

Taking into account the considerations in Remark 1, a constraint of the following form can be used:

$$0 < S^{min} \le S_k \le S^{max} \le 1. \tag{18}$$

- *SC voltage.* Due to technological aspects, the operating voltage limits of SCs need to be bounded in a specific range. Such bounds can be expressed as $v_{bus,k} \in [v_{bus}^{min}, v_{bus}^{max}]$ which in turn are equivalent to the corresponding bounds on the stored energy, i.e.,

$$E_{bus}^{min} \le E_{bus,k} \le E_{bus}^{max}, \tag{19}$$

where $E_{bus}^{[min|max]} = \frac{1}{2} C v_{bus}^{[min|max]2}$.

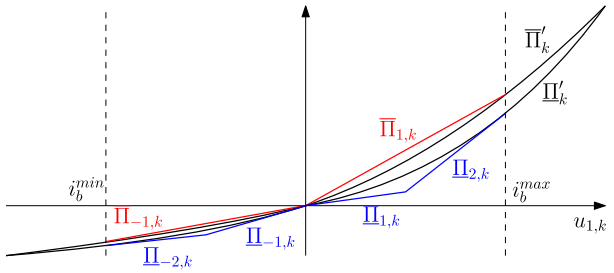

Fig. 6. Piecewise affine lower (blue) and upper (red) bounds to Π_k.

- *DC-DC voltage gains.* As stated in Section II, the first conversion stage is characterized by $M_1 < 1$. Since the PV panel is operated at $(v_{pv}^+[P_{pv}], i_{pv}^+[P_{pv}])$, it holds that $v_{pv}(t) \ge v_{MPP}$ (see Fig. 2) and therefore $M_1 < 1$ is guaranteed if $v_{bus}^{max} < v_{MPP}$, where the MPP is evaluated for maximal irradiance/temperature conditions. As for the second stage, $M_2 > 1$ is ensured if $v_{oc}^{min} - R|i_b^{min}| > v_{bus}^{max}$. The above two constraints can be satisfied by a suitable design of the electrical components.

It turns out that, while constraints (16), (18), (19) are linear in the state and input variables of (14), constraints (15) are not, due to the dependence of $P_{pv,k}$ on $u_{1,k}$ and $v_{oc}(S_k)$ (see (13b)). Such constraints can be tackled by devising suitable piecewise affine bounds to the involved quantities as follows. Let us define $\Pi_k = R u_{1,k}^2 + v_{oc}(S_k) u_{1,k}$. By (13b), (15) reads

$$-\Pi_k \le u_{2,k} \le P_{MPP,k} - \Pi_k. \tag{20}$$

By the considerations in Remark 1, Π_k can be bounded above and below for $i_b^{min} \le u_{1,k} \le i_b^{max}$ by

$$\overline{\Pi}'_k \triangleq \begin{cases} R u_{1,k}^2 + v_{oc}^{min} u_{1,k}, & i_b^{min} \le u_{1,k} \le 0 \\ R u_{1,k}^2 + v_{oc}^{max} u_{1,k}, & 0 \le u_{1,k} \le i_b^{max} \end{cases} \tag{21}$$

and

$$\underline{\Pi}'_k \triangleq \begin{cases} R u_{1,k}^2 + v_{oc}^{max} u_{1,k}, & i_b^{min} \le u_{1,k} \le 0 \\ R u_{1,k}^2 + v_{oc}^{min} u_{1,k}, & 0 \le u_{1,k} \le i_b^{max}, \end{cases} \tag{22}$$

respectively, and hence, at the price of a slight amount of conservatism, (20) holds if

$$-\underline{\Pi}'_k \le u_{2,k} \le P_{MPP,k} - \overline{\Pi}'_k. \tag{23}$$

Clearly, the wider the interval $[v_{oc}^{min}, v_{oc}^{max}]$, the more (23) is conservative with respect to (20). Note that the right constraint in (23) is convex, being $\overline{\Pi}'_k$ a convex function of $u_{1,k}$, while the left one is not. In order to devise an optimization problem enjoying properties that allow its solution to the global optimum, a piecewise affine lower bound $\underline{\Pi}_k$ to $\underline{\Pi}'_k$ can be exploited. In this respect, many choices are indeed possible and $\underline{\Pi}'_k$ can be approximated with arbitrary precision at the price of increasing the computational complexity of the resulting mixed-integer program. However, for the sake of simplicity, we opt for the following lower bound which holds if (17) is in place (see Fig. 6):

$$\underline{\Pi}_k \triangleq \begin{cases} \underline{\Pi}_{-2,k} \triangleq \left(2R i_b^{min} + v_{oc}^{max}\right) u_{1,k} - R i_b^{min\,2}, & i_b^{min} \le u_{1,k} \le \frac{i_b^{min}}{2} \\ \underline{\Pi}_{-1,k} \triangleq v_{oc}^{max} u_{1,k}, & \frac{i_b^{min}}{2} \le u_{1,k} \le 0 \\ \underline{\Pi}_{1,k} \triangleq v_{oc}^{min} u_{1,k}, & 0 \le u_{1,k} \le \frac{i_b^{max}}{2} \\ \underline{\Pi}_{2,k} \triangleq \left(2R i_b^{max} + v_{oc}^{min}\right) u_{1,k} - R i_b^{max\,2}, & \frac{i_b^{max}}{2} \le u_{1,k} \le i_b^{max} \end{cases} \tag{24}$$

Concerning the right constraint in (23), despite its convexity, we choose to exploit a piecewise linear upper bound $\overline{\Pi}_k$ to

$\overline{\Pi'}_k$. This is done to avoid having to deal with a quadratically constrained mixed-integer problem, which is much harder to solve than a MILP. Such bound can be computed (see Fig. 6) as

$$\overline{\Pi}_k \triangleq \begin{cases} \overline{\Pi}_{-1,k} \triangleq \left(Ri_b^{min} + v_{oc}^{min}\right)u_{1,k}, \; i_b^{min} \le u_{1,k} \le 0 \\ \overline{\Pi}_{1,k} \triangleq \left(Ri_b^{max} + v_{oc}^{max}\right)u_{1,k}, \;\; 0 \le u_{1,k} \le i_b^{max}. \end{cases}$$

Using $\overline{\Pi}_k$ and $\underline{\Pi}_k$ as upper and lower bounds to Π_k, it turns out that (20), and in turn (15), holds if there exist binary variables $z_{-2,k}, z_{-1,k}, z_{1,k}, z_{2,k}$ such that

$$z_{-2,k}, z_{-1,k}, z_{1,k}, z_{2,k} \in \{0, 1\} \tag{25a}$$
$$z_{-2,k} + z_{-1,k} + z_{1,k} + z_{2,k} = 1 \tag{25b}$$
$$W_{i,k} = W\left(1 - z_{i,k}\right), \quad i = -2, -1, 1, 2 \tag{25c}$$
$$u_{1,k} \le \frac{i_b^{min}}{2} + W_{-2,k} \tag{25d}$$
$$-W_{-1,k} + \frac{i_b^{min}}{2} \le u_{1,k} \le W_{-1,k} \tag{25e}$$
$$-W_{1,k} \le u_{1,k} \le \frac{i_b^{max}}{2} + W_{1,k} \tag{25f}$$
$$-W_{2,k} + \frac{i_b^{max}}{2} \le u_{1,k} \tag{25g}$$
$$-W_{-2,k} - \underline{\Pi}_{-2,k} \le u_{2,k} \le P_{MPP,k} - \overline{\Pi}_{-1,k} + W_{-2,k} \tag{25h}$$
$$-W_{-1,k} - \underline{\Pi}_{-1,k} \le u_{2,k} \le P_{MPP,k} - \overline{\Pi}_{-1,k} + W_{-1,k} \tag{25i}$$
$$-W_{1,k} - \underline{\Pi}_{1,k} \le u_{2,k} \le P_{MPP,k} - \overline{\Pi}_{1,k} + W_{1,k} \tag{25j}$$
$$-W_{2,k} - \underline{\Pi}_{2,k} \le u_{2,k} \le P_{MPP,k} - \overline{\Pi}_{1,k} + W_{2,k}. \tag{25k}$$

In (25), a standard big-M argument is used to represent the piecewise linear bounds $\underline{\Pi}_k$ and $\overline{\Pi}_k$. The constant W must be chosen large enough that when $W_{i,k}$ is nonzero, the constraints involving it become trivial (note that W can be estimated from the bounds on the quantities involved in such constraints). The binary variables $z_{-2,k}, z_{-1,k}, z_{1,k}, z_{2,k}$ indicate which of the intervals in (24) $u_{1,k}$ belongs to as per (25d)–(25g), so that the corresponding constraint in (25h)–(25k) is enforced. Note that (25a)–(25c) allow one and only one $z_{i,k}$, $i \in \{-2, -1, 1, 2\}$ to be 1 and the corresponding $W_{i,k}$ to be zero. Concerning the objective function to be optimized, the minimization of battery strain due to charging/discharging is well captured by the $1-$norm of the current time series $i_{b,k} = u_{1,k}$, i.e.,

$$J_T = \sum_{k=0}^{T-1} |u_{1,k}| \tag{26}$$

(see [8]). In light of the above points, the optimal control problem can be formulated as follows:

Problem 1:

$$\Theta^* = \arg\min_{\Theta} \sum_{k=0}^{T-1} h_k$$

subjected to:

(14), (16), (18), (19), (25), $k = 0, \ldots, T-1$

$$-h_k \le u_{1,k} \le h_k, \;\; k = 0, \ldots, T-1 \tag{27a}$$
$$\left(S_0, E_{bus,0}\right) = \left(S^0, E_{bus}^0\right) \tag{27b}$$
$$\left(S_T, E_{bus,T}\right) = \left(S^T, E_{bus}^T\right), \tag{27c}$$

where the optimization variables are represented by the set of sequences

$$\Theta = \Big\{\left(u_{1,k}, u_{2,k}, h_k\right), \quad k = 0, \ldots T-1, \\ \left(z_{-2,k}, z_{-1,k}, z_{1,k}, z_{2,k}\right), \quad k = 0, \ldots T-1, \\ \left(S_k, E_{bus,k}\right), \quad k = 0, \ldots T\Big\}.$$

Notice that the slack variables h_k introduced in (27a) allow one to formulate the objective function J_T in a linear fashion, while the two constraints in (27b)–(27c) are used to enforce boundary conditions on the two state variables, for given values of $S^0, E_{bus}^0, S^T, E_{bus}^T$. Problem 1 is a MILP involving $4T$ binary variables. However, its computational complexity is heavily mitigated by the complementarity constraint $z_{-2,k} + z_{-1,k} + z_{1,k} + z_{2,k} = 1$, which is exploited very efficiently by modern solvers even for quite large instances.

The command signals $M_1(t)$ and $M_2(t)$ corresponding to the optimal solution can be constructed from the ZOH-maintained versions of the optimal sequences in Θ^* via (13), (11), (10) as described at the beginning of this section.

IV. Numerical Results

In this section, a simulation study is conducted to evaluate the performance and computational feasibility of the proposed method. The considered setup consists of an islanded system modeled as in Section II. The ESS is composed by the parallel of 2 series of 9 new $LiFePO_4$ cells with the characteristics taken from [14], for a maximum open circuit voltage of $26V$ and a total stored charge of $6Ah$. Forecasts of solar irradiance $G(t)$ and temperature $T_c(t)$ are taken from the publicly available data set in [9] and refer to a summer day in Australia. The sampling time is chosen as $\tau_s = 15$ min. By using these data, the PV peak power generation forecast time series $P_{MPP,k}$ is computed numerically by exploiting (1), assuming a 65W PV module whose parameters are extracted according to the methods in [20]. The SC bus is composed by the parallel of 4 series of 4 super-capacitors rated $4000F/3.2V$, thus resulting in a single equivalent SC with $4000F/12.8V$. A feasible load profile forecast $P_{l,k}$ is considered.

In order avoid thermal stress on the components, the following constraints are enforced on the battery charging/discharging current and on the SC bus:

$$i_b^{min} = -3A, \quad i_b^{max} = 3A, \quad v_{bus}^{min} = 7V, \quad v_{bus}^{max} = 12V.$$

Bounds $v_{oc}^{min}, v_{oc}^{max}$ are chosen as $[v_{oc}^{min}, v_{oc}^{max}] = [v^{cut}, v_{oc}(1)]$, yielding the most conservative bound (23) as per Remark 1, with S^{min}, S^{max} set accordingly. Boundary conditions on the battery SOC and SC voltage are set as $S^0 = S^T = 0.5$, $v_{bus}^0 = v_{bus}^T = 9.8V$. This guarantees the same initial SOC at the beginning of consecutive days. Of course, different choices could be considered on the basis, e.g., of generation and load forecasts over time periods spanning multiple days. An instance of Problem 1 was run over a time horizon of one day, thus involving 482 continuous and 384 binary variables. Solver time averaged over 100 runs turned out to be 0.54 seconds.[1] The continuous-time model (5) was simulated using the control inputs computed from the obtained optimal solution. Fig. 7 depicts the evolution of the most relevant

[1] Simulations have been performed using Gurobi [21] on a 3.49 GHz Apple M2 processor. Tolerance for primal and dual feasibility is 10^{-6}, while the integrality tolerance is 10^{-5}.

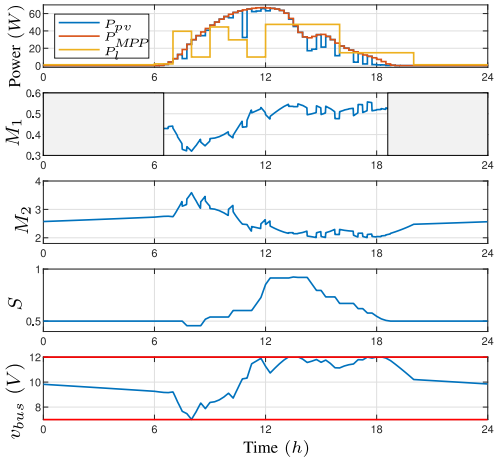

Fig. 7. Evolution of PV panel power output P_{pv}(t), DC-DC gains $M_1(t)$, M_2(t), battery state of charge S(t), and SC voltage v_{bus}(t). In the first plot, P_{pv}(t) is compared with the peak power P_{MPP}(t) corresponding to irradiance G(t) and temperature T_c(t), and with load power P_l(t). Gray regions in the plot of M_1 correspond to time intervals where PV generation is negligible and PV side converter is switched off.

variables. The generated power $P_{pv,k}$ satisfies $P_{pv,k} \leq P_{MPP,k}$ as expected. It is worth noticing that, when required by the load profile, the optimal control action actually drives $P_{pv,k}$ extremely close to $P_{MPP,k}$, thus showing a very low level of conservatism of the piecewise affine constraints (25) with respect to the nonlinear ones (20). From the plot of v_{bus}, one may notice that the SC is charged/discharged several times and spans the entire allowed range, as opposite to the battery SOC S that basically exhibits only one partial charging/discharging cycle. Such a behavior is in line with the objective function of Problem 1 which aims at reducing battery cycles.

The proposed approach has been compared with the standard charging technique consisting of MPPT operation combined with constant current charging. The latter has been adapted to deal with the presence of load, and controller parameters have been tuned by trial-and-error in order to satisfy the same constraints as the optimal control problem. The proposed approach outperforms this benchmark in terms of the battery strain J_T in (26), reducing it by about 30%.

Finally, it is worth noticing that this problem instance admits a solution also assuming a 7-year-old battery, by considering the relevant values of the parameters. However, if different constraints are considered, infeasibility may occur in the latter case mainly due to more stringent requirements on S^{min}. For example, the bound $S^0 = S^T$ can be decreased down to 0.22 for a new battery without incurring infeasibility, while for a 7-year-old one only values down to 0.37 are tolerated.

V. Conclusion

In this letter, a novel control scheme for optimal operation of electrical storage systems connected to a PV power source has been introduced, by exploiting an architecture consisting of two DC-DC converters connected through a super-capacitor bus. The proposed framework is aimed at satisfying power and technological constraints while optimizing battery cycles, and considers realistic circuit models. By means of suitable model transformations and nonconvex constraint handling using piecewise-affine bounds, the underlying optimization problem has been formulated as a computationally tractable MILP. The performance of the proposed method has been evaluated by numerical simulations. Future work will focus on the adaptation of the proposed control architecture to online feedback MPC, as well as on a robust formulation accounting for uncertainties affecting the load and generation profiles.

References

[1] C. S. Lai, Y. Jia, L. L. Lai, Z. Xu, M. D. McCulloch, and K. P. Wong, "A comprehensive review on large-scale photovoltaic system with applications of electrical energy storage," *Renew. Sustain. Energy Rev.*, vol. 78, pp. 439–451, Oct. 2017.

[2] M. M. Rana, M. Uddin, M. R. Sarkar, G. M. Shafiullah, H. Mo, and M. Atef, "A review on hybrid photovoltaic—battery energy storage system: Current status, challenges, and future directions," *J. Energy Storage*, vol. 51, Jul. 2022, Art. no. 104597.

[3] A. Gurung and Q. Qiao, "Solar charging batteries: Advances, challenges, and opportunities," *Joule*, vol. 2, no. 7, pp. 1217–1230, 2018.

[4] F. Corti et al., "Dynamic analysis of a supercapacitor DC-link in photovoltaic conversion applications," *Energies*, vol. 16, no. 16, p. 5864, 2023.

[5] K. Chen, S. Tian, Y. Cheng, and L. Bai, "An improved MPPT controller for photovoltaic system under partial shading condition," *IEEE Trans. Sustain. Energy*, vol. 5, no. 3, pp. 978–985, Jul. 2014.

[6] A. Mohapatra, B. Nayak, P. Das, and K. B. Mohanty, "A review on MPPT techniques of PV system under partial shading condition," *Renew. Sustain. Energy Rev.*, vol. 80, pp. 854–867, Dec. 2017.

[7] P. K. Pathak and A. K. Yadav, "Design of battery charging circuit through intelligent MPPT using SPV system," *Sol. Energy*, vol. 178, pp. 79–89, Jan. 2019.

[8] N. Collath, B. Tepe, S. Englberger, A. Jossen, and H. Hesse, "Aging aware operation of lithium-ion battery energy storage systems: A review," *J. Energy Storage*, vol. 55, Nov. 2022, Art. no. 105634.

[9] E. L. Ratnam, S. R. Weller, C. M. Kellett, and A. T. Murray, "Residential load and rooftop PV generation: An Australian distribution network dataset," *Int. J. Sustain. Energy*, vol. 36, no. 8, pp. 787–806, 2017.

[10] W. De Soto, S. A. Klein, and W. A. Beckman, "Improvement and validation of a model for photovoltaic array performance," *Sol. Energy*, vol. 80, no. 1, pp. 78–88, 2006.

[11] J. C. Blakesley, F. A. Castro, G. Koutsourakis, A. Laudani, G. M. Lozito, and F. R. Fulginei, "Towards non-destructive individual cell I-V characteristic curve extraction from photovoltaic module measurements," *Sol. Energy*, vol. 202, pp. 342–357, May 2020.

[12] S. Amir, M. Gulzar, M. O. Tarar, I. H. Naqvi, N. A. Zaffar, and M. G. Pecht, "Dynamic equivalent circuit model to estimate state-of-health of lithium-ion batteries," *IEEE Access*, vol. 10, pp. 18279–18288, 2022.

[13] S. Nejad, D. T. Gladwin, and D. A. Stone, "A systematic review of lumped-parameter equivalent circuit models for real-time estimation of lithium-ion battery states," *J. Power Sources*, vol. 316, pp. 183–196, Jun. 2016.

[14] T.-J. Kuo et al., "State of charge modeling of lithium-ion batteries using dual exponential functions," *J. Power Sources*, vol. 315, pp. 331–338, May 2016.

[15] L. Ju, P. Long, G. Geng, and Q. Jiang, "Open circuit voltage—State of charge curve calibration by redefining max–min bounds for lithium-ion batteries," *J. Energy Storage*, vol. 79, Feb. 2024, Art. no. 110224.

[16] M. K. Kazimierczuk, *Pulse-Width Modulated DC-DC Power Converters*. Hoboken, NJ, USA: Wiley, 2015.

[17] M. K. Kazimierczuk, D. K. Saini, and A. Ayachit, *Average Current-Mode Control of DC-DC Power Converters*. Hoboken, NJ, USA: Wiley, 2022.

[18] V. Rajini and M. Anand, "Investigations on interleaved and coupled split-pi DC-DC converter for hybrid electric vehicle applications," *Int. J. Renew. Energy Res.*, vol. 11, no. 2, pp. 808–817, 2021.

[19] Y. Elthokaby, I. Abdelsalam, N. Abdel-Rahim, and I. Mohamed, "Standalone PV-based single-phase split-source inverter using model-predictive control," *Alexandria Eng. J.*, vol. 62, pp. 357–367, Jan. 2023.

[20] A. Laudani, F. R. Fulginei, and A. Salvini, "Identification of the one-diode model for photovoltaic modules from datasheet values," *Sol. Energy*, vol. 108, pp. 432–446, Oct. 2014.

[21] "Gurobi optimizer reference manual." Gurobi optimization, LLC. 2024. [Online]. Available: https://www.gurobi.com